processes

MDPI

Article

Dynamic Response Analysis of Control Loops in an Electro-Hydraulic Servo Pump Control System

Wenguang Jiang [1], Pengshuo Jia [1], Guishan Yan [1], Gexin Chen [1,2,*], Chao Ai [1], Tiangui Zhang [1], Keyi Liu [2], Chunyu Jia [1] and Wei Shen [3]

[1] School of Mechanical Engineering, Yanshan University, Qinhuangdao 066004, China
[2] Mechanical and Electrical Engineering, Xinjiang Institute of Engineering, Urumqi 830023, China
[3] China Railway Shanhaiguan Bridge Croup Co., Ltd., Qinhuangdao 066200, China
* Correspondence: jygxchen@ysu.edu.cn; Tel.: +86-335-805-7100

Abstract: An electro-hydraulic servo pump control system realizes the basic action of a hydraulic cylinder by controlling the servo motor, which effectively improves the problems of a traditional valve control system such as high energy consumption, low power-to-weight ratio, and poor anti-pollution ability. However, the static accuracy and dynamic performance of an electro-hydraulic servo pump control system are limited due to the electro-hydraulic coupling and flow nonlinearity. Based on this, in this paper, we establish a mathematical model of an electro-hydraulic servo pump control system. Starting from the internal control mechanism of the system, the Simulink simulation model is established to analyze the dynamic response of the system current loop, speed loop, position loop, and pressure loop. The system parameters are obtained by combining the system dynamic analysis and component technology samples. The position/force control model of the electro-hydraulic servo pump control system is built for simulation, and the experimental platform is built for experimental verification. The results show that the system position/force control can achieve good dynamic response and steady-state accuracy after the parameters are determined based on the dynamic analysis of control loops.

Keywords: electro-hydraulic servo pump control system; control loop; dynamic characteristics; position/force control; simulation analysis; experimental verification

Citation: Jiang, W.; Jia, P.; Yan, G.; Chen, G.; Ai, C.; Zhang, T.; Liu, K.; Jia, C.; Shen, W. Dynamic Response Analysis of Control Loops in an Electro-Hydraulic Servo Pump Control System. *Processes* **2022**, *10*, 1647. https://doi.org/10.3390/pr10081647

Academic Editor: Jiaqiang E

Received: 20 June 2022
Accepted: 16 August 2022
Published: 19 August 2022

1. Introduction

An electro-hydraulic servo pump control system adjusts the flow and pressure of the system by controlling the servo motor, and then controls the output of the hydraulic cylinder. As compared with a traditional valve control system, the system eliminates the huge hydraulic station, complex pipelines, and expensive servo valve, effectively overcoming the technical defects of electro-hydraulic servo valve control technology such as poor anti-pollution ability, low integration, and serious energy waste. It has the technical advantages of a system that has high efficiency and energy savings, a high power-to-weight ratio, and is environmentally friendly [1,2]. As early as 1967, Herbert E. Merritt in America discussed the analysis and design of hydraulic control system. The nonlinear characteristics which may appear in the hydraulic control system and their influence on the system were analyzed [3]. Kazuo Nakano and Yutaka Tanaka in Japan first proposed a constant pressure control scheme using a variable frequency motor to drive the hydraulic system [4]. Japanese YUKEN used a bidirectional stepless speed regulation motor to drive a quantitative axial piston pump and developed an IH servo control unit, which realized bidirectional stepless regulation of the hydraulic pump [5]. The servo-driven UPS series energy-saving hydraulic unit developed by the Fujikoshi Company in Japan saved about 60% energy compared with ordinary hydraulic systems [6]. Europe and America also successfully applied the pump control system to Airbus A380 as a backup actuation system [7]. Since 1997, the

American Moog company has successively installed its new electro-hydraulic servo pump control system on the F18 fighter, C130, F16, C141, and other aircraft or simulators, and has conducted relevant experiments [8,9]. The very new Airbus product generation, A380 and A400M, now features a mixed flight control actuation power source distribution, associating conventional FBW hydraulic actuators with electrically powered actuators [10]. By the 21st century, EHA actuators were adopted in the main flight control rudder surface of all American F35 fighter aircrafts [11]. In addition, there is an Electric Drive Design Initiative in the United States, which aims to develop new EHA to gain technological leadership in future multi-electric and all-electric aircraft [12]. Fu J proposed new approaches to enable incremental modelling, thermal balance analysis, response to free-run or jamming faults, impact of compliance on parasitic motion, and influence of temperature. A special focus is placed on friction and compliance of the mechanical transmission with fault injection and temperature dependence. Aileron actuation is used to highlight the proposals for control design, energy consumption and thermal analysis, power network pollution analysis, and fault response [13]. N Vasiliu illustrated numerical simulation of fluid power systems by LMS Amesim Platform covering hydrostatic transmissions, electrohydraulic servo valves, hydraulic servomechanisms for aerospace engineering, speed governors for power machines, fuel injection systems, and automotive servo systems [14].

However, with the gradual expansion of the application field of electro-hydraulic servo pump control technology, industrial equipment has higher and higher requirements on the output accuracy of the system, and the influence of system multi-variables, strong electro-hydraulic coupling, flow nonlinear, and other factors on the control accuracy and response speed of the system are also more and more obvious [15,16]. In recent years, great progress has been made in software and hardware research on electro-hydraulic servo pump control systems. Daniel Gorges, from the Technical University of Kaiserslautern in Germany, proposed an adaptive robust force control method, which effectively improved the high-precision force control characteristics of the electro-hydraulic servo pump control system [17]. Dao Thanh Liem, from Ulsan University in South Korea, proposed a feedforward neural network fuzzy predictor and optimized the PID parameters online, which effectively reduced the overshoot and improved the dynamic response characteristics of the system [18]. Deticek et al., from University of Ljubljana, proposed a flexible switching strategy for servo motors of pump control system, which overcame the problem of high-frequency commutation control of a rotor with large inertia [19]. Chong Chee Soon et al., from the Malaysian University of Technology, adopted the fuzzy logic controller optimized by particle swarm optimization to control the position of the electro-hydraulic servo pump control system and achieved accurate tracking of the reference trajectory within a certain range [20]. Ryoya Suzuki, from the University of Tokyo in Japan, designed a vane pump made of ceramic material, which effectively reduced the internal leakage of the pump and significantly improved the position control accuracy of the system [21]. Tianyi Ko, from the University of Tokyo in Japan, analyzed the influence of viscosity loss and internal leakage loss of the electro-hydraulic servo pump control system on the control performance of the system, and effectively improved the power-weight ratio and control performance of the system by reducing the internal clearance of the system and expanding the force area [22]. G Altare presented and described an innovative design solution for a compact Electro-Hydraulic Actuator (EHA). In particular, a novel pressure compensation system was formulated to minimize power losses associated with the internal lubricating gaps in the whole field of operation. The paper details the numerical modelling of the system, showing results which describe its main features of operation [23].

Fu Yongling et al., from the Beijing University of Aeronautics and Astronautics, proposed a sliding mode variable structure control algorithm under variable load conditions [24] and designed a nonlinear proportional integral position controller to compensate for the adverse effects caused by viscosity and to improve the position accuracy of electro-hydrostatic actuators [25]. Jiao Zongxia et al., from the Beijing University of Aeronautics and Astronautics, improved the dynamic characteristics of an electro-hydraulic servo pump control system by improving the output torque of the motor, reducing the rotational inertia of the motor pump group, adopting the structure of the double motor pump group, and finally realized the high-precision control of the system [26].

In this paper, taking the electro-hydraulic servo pump control system as the main research object, we study the position/force control performance of the system. The working principle of an electro-hydraulic servo pump control system is introduced in detail and a nonlinear mathematical model of the system is established. In view of the problem that the control performance of the system is limited by factors such as multivariable, electro-mechanical, and hydraulic strong coupling and flow nonlinearity, the dynamic response characteristics of each control loop in the system are analyzed, and the system parameters are determined based on the technical samples of components. Finally, through Simulink simulation and experimental research, it is verified that the electro-hydraulic servo pump control system can achieve a good position/force control effect.

2. Principle of an Electro-Hydraulic Servo Pump Control System

The system adopts an integrated volume control scheme of a servo motor, quantitative pump, and hydraulic cylinder. The basic working principle diagram is shown in Figure 1.

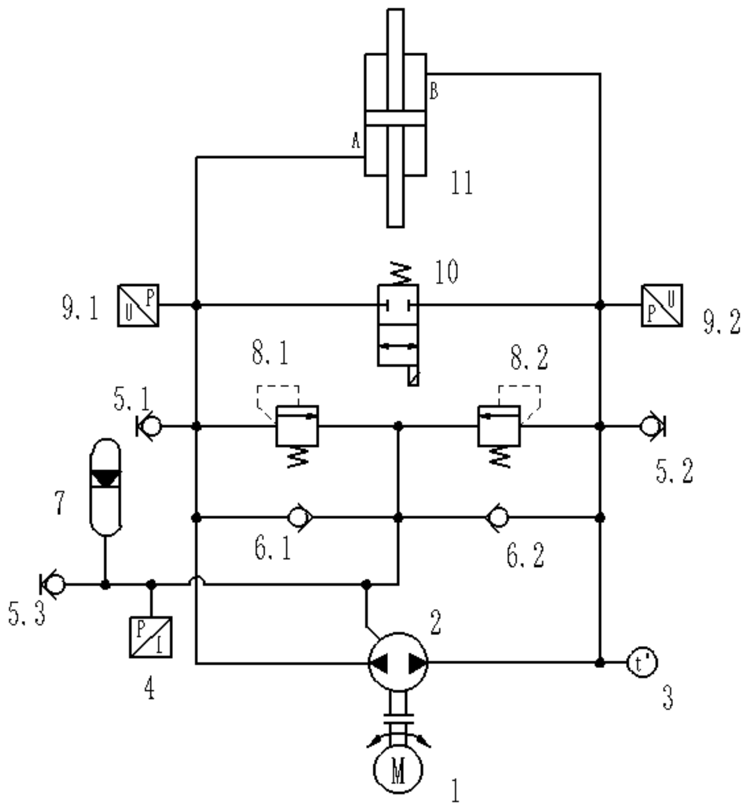

Figure 1. Schematic diagram of the DDVC electro-hydraulic servo system. 1, servo motor; 2, positive displacement pump; 3, temperature sensor; 4, pressure relay; 5, pressure joint; 6, check valve; 7, oil replenishment accumulator; 8, relief valve; 9, pressure sensor; 10, unloading valve; 11, symmetrical hydraulic cylinder.

The system adopts a servo motor to drive the quantitative pump coaxially. The suction and discharge ports of the quantitative pump are directly connected with the two load ports of the hydraulic cylinder. The accumulator is used with a one-way valve to replenish the oil in the system. The controller controls the speed and torque of the servo motor through output control instructions and adjusts the displacement and force of the hydraulic cylinder.

3. System Mathematical Model

3.1. Servo Motor Control Unit

The AC servo motor is responsible for converting the input voltage into the output speed and torque of the motor. The mathematical equation of the motor can be expressed as follows:

$$\begin{cases} U_{\mathrm{q}} = R_{\mathrm{s}} i_{\mathrm{q}} + L_{\mathrm{q}} \dfrac{\mathrm{d}}{\mathrm{d}t} i_{\mathrm{q}} + \omega_{\mathrm{m}} K_{\mathrm{e}} \\ T_{\mathrm{e}} = K_{\mathrm{t}} i_{\mathrm{q}} \\ T_{\mathrm{L}} = D_{\mathrm{p}} P_{\mathrm{L}} \\ T_{\mathrm{e}} - T_{\mathrm{L}} = J_{\mathrm{m}} \dfrac{\mathrm{d}\omega_{\mathrm{m}}}{\mathrm{d}t} + B_{\mathrm{m}} \omega_{\mathrm{m}} \end{cases} \tag{1}$$

where U_{q} is the q axis voltage, R_{s} is the motor winding resistance, L_{q} is the q axis inductance, i_{q} is the q axis current, ω_{m} is the motor output speed, K_{e} is the permanent magnet inverse electromotive force coefficient, T_{e} is the motor torque, K_{t} is the motor torque coefficient, T_{L} is the hydraulic pump load torque, D_{p} is the hydraulic pump displacement, P_{L} is the pressure difference between two cavities of hydraulic pump system, J_{m} is the moment of inertia of motor pump, and B_{m} is the friction coefficient of the motor pump combination.

3.2. Fixed Displacement Radial Piston Pump

Considering the factors of oil compression and internal and external leakage, the flow distribution characteristics of the quantitative pump were analyzed as shown in Figure 2.

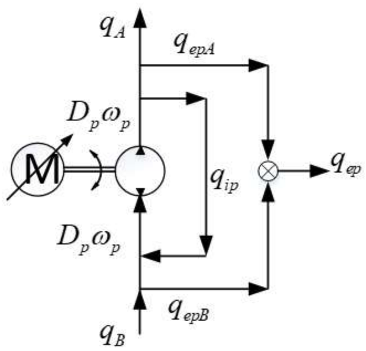

Figure 2. Flow distribution of the hydraulic pump.

The two-chamber load volume flow from the pump to the controlled hydraulic cylinder can be expressed as:

$$\begin{cases} q_{\mathrm{A}} = D_{\mathrm{p}}\omega_{\mathrm{p}} - C_{\mathrm{ip}}(p_{\mathrm{A}} - p_{\mathrm{B}}) - C_{\mathrm{ep}} p_{\mathrm{A}} \\ q_{\mathrm{B}} = D_{\mathrm{p}}\omega_{\mathrm{p}} - C_{\mathrm{ip}}(p_{\mathrm{A}} - p_{\mathrm{B}}) + C_{\mathrm{ep}} p_{\mathrm{B}} \end{cases} \tag{2}$$

Further, the continuous equation of load flow of the quantitative pump can be expressed as:

$$Q_{\mathrm{p}} = D_{\mathrm{p}}\omega_{\mathrm{m}} - C_{\mathrm{p}} P_{\mathrm{L}} \tag{3}$$

where q_{A} and q_{B} are the flows of system chamber A and B, respectively; C_{ip} and C_{ep} are the internal and external leakage coefficients of the pump, respectively; p_{A} is the pressure of system chamber A; and p_{B} is the pressure of system chamber B, $q_{\mathrm{ip}} = C_{\mathrm{ip}}(p_{\mathrm{A}} - p_{\mathrm{B}})$, $q_{\mathrm{epA}} = C_{\mathrm{ep}} p_{\mathrm{A}}$, $q_{\mathrm{epB}} = C_{\mathrm{ep}} p_{\mathrm{B}}$, $Q_{\mathrm{p}} = \dfrac{q_{\mathrm{A}} + q_{\mathrm{B}}}{2}$, $C_{\mathrm{p}} = C_{\mathrm{ip}} + \dfrac{1}{2} C_{\mathrm{ep}}$.

3.3. Double-Acting Symmetrical Hydraulic Cylinder

Considering load conditions, oil compression, internal and external leakage, and other factors, the flow distribution characteristics of the hydraulic cylinder were analyzed as shown in Figure 3.

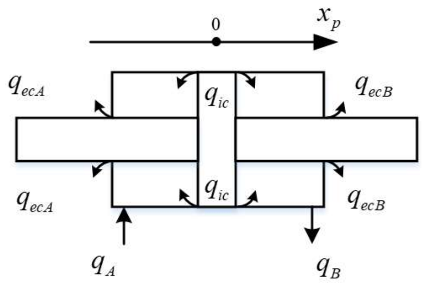

Figure 3. Hydraulic cylinder flow distribution.

The flow continuity equation of cavities A and B of the hydraulic cylinder is:

$$\begin{cases} q_{\mathrm{A}} = A\dot{x}_{\mathrm{p}} + C_{\mathrm{ic}}(p_{\mathrm{A}} - p_{\mathrm{B}}) + C_{\mathrm{ec}}p_{\mathrm{A}} + \dfrac{V_0 + Ax_{\mathrm{p}}}{\beta_{\mathrm{e}}}\dot{p}_{\mathrm{A}} \\ q_{\mathrm{B}} = A\dot{x}_{\mathrm{p}} + C_{\mathrm{ic}}(p_{\mathrm{A}} - p_{\mathrm{B}}) - C_{\mathrm{ec}}p_{\mathrm{B}} - \dfrac{V_0 - Ax_{\mathrm{p}}}{\beta_{\mathrm{e}}}\dot{p}_{\mathrm{B}} \end{cases} \tag{4}$$

Further, the continuity equation of load flow of the symmetrical hydraulic cylinder can be expressed as:

$$Q_{\mathrm{p}} = A_{\mathrm{p}}\dot{x}_{\mathrm{p}} + K_{\mathrm{ce}}P_{\mathrm{L}} + \frac{V_{\mathrm{t}}}{4\beta_{\mathrm{e}}}\dot{P}_{\mathrm{L}} \tag{5}$$

where A_{p} is the effective working area of the double-acting symmetrical hydraulic cylinder, x_{p} is the displacement of the hydraulic cylinder, C_{ic} is the internal leakage coefficient of hydraulic cylinder, C_{ec} is the external leakage coefficient of hydraulic cylinder, β_{e} is the effective volume elastic modulus, and V_0 is the volume of each working chamber when the piston is in the middle position of the hydraulic cylinder, $q_{\mathrm{ic}} = C_{\mathrm{ic}}(p_{\mathrm{A}} - p_{\mathrm{B}})$, $q_{\mathrm{ecA}} = C_{\mathrm{ec}}p_{\mathrm{A}}$, $q_{\mathrm{ecB}} = C_{\mathrm{ec}}p_{\mathrm{B}}$, $K_{\mathrm{ce}} = C_{\mathrm{ic}} + \frac{1}{2}C_{\mathrm{ec}}$, $V_{\mathrm{t}} = 2V_0$.

When the piston position of the double-acting symmetrical cylinder is in the middle position ($x_{\mathrm{p}} = 0$), the hydraulic spring stiffness is the lowest, the corresponding hydraulic system natural frequency is the lowest, and the stability is the worst. Therefore, this point was selected for research.

According to Newton's second law, the force balance equation of the hydraulic cylinder was deduced as follows:

$$A_{\mathrm{p}}(p_{\mathrm{A}} - p_{\mathrm{B}}) = m_{\mathrm{t}}\ddot{x}_{\mathrm{p}} + B_{\mathrm{p}}\dot{x}_{\mathrm{p}} + Kx_{\mathrm{p}} + F_{\mathrm{L}} \tag{6}$$

where m_{t} is the total mass of the piston and the load converted onto the piston, B_{p} is the viscous damping coefficient, K is the equivalent spring stiffness of the load, and F_{L} is the external interference of the system and friction force.

4. Control Characteristics Analysis of the Electro-Hydraulic Servo Pump Control System

In this paper, the position control of the electro-hydraulic servo pump control system adopts three closed-loop control schemes, including the position loop, servo motor speed loop, and current loop, from outside to inside, as shown in Figure 4.

Usually, the current of the servo motor produces torque, which causes the speed of the quantitative pump driven by the servo motor to change, and finally causes the position of the hydraulic cylinder to change.

When the system performs force control, the servo motor controls the torque directly through the current loop, using the torque direct drive control scheme by adjusting the current input to change the hydraulic torque, and finally causing the pressure in the hydraulic cylinder load chamber to change, thus achieving high performance control of the system pressure. The system is successively composed of a system pressure loop and a current loop, from outside to inside, forming a double loop control structure, as shown in Figure 5.

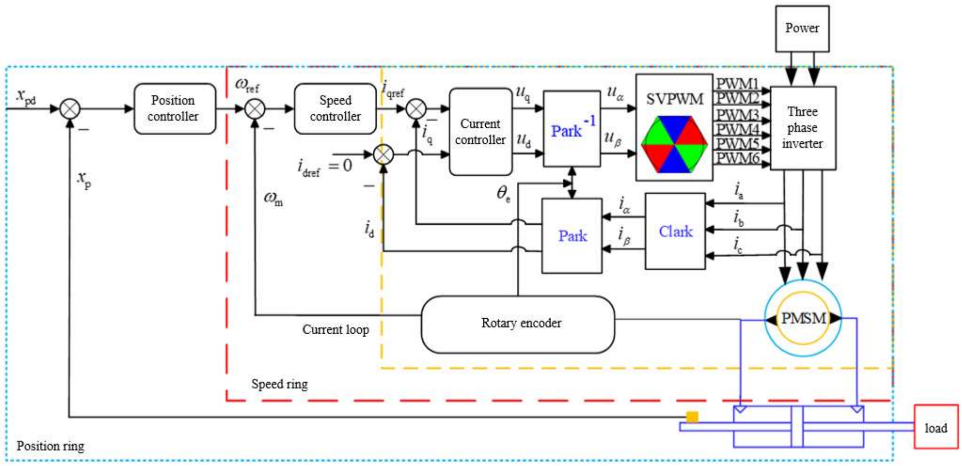

Figure 4. Position control three-loop diagram of the pump control system.

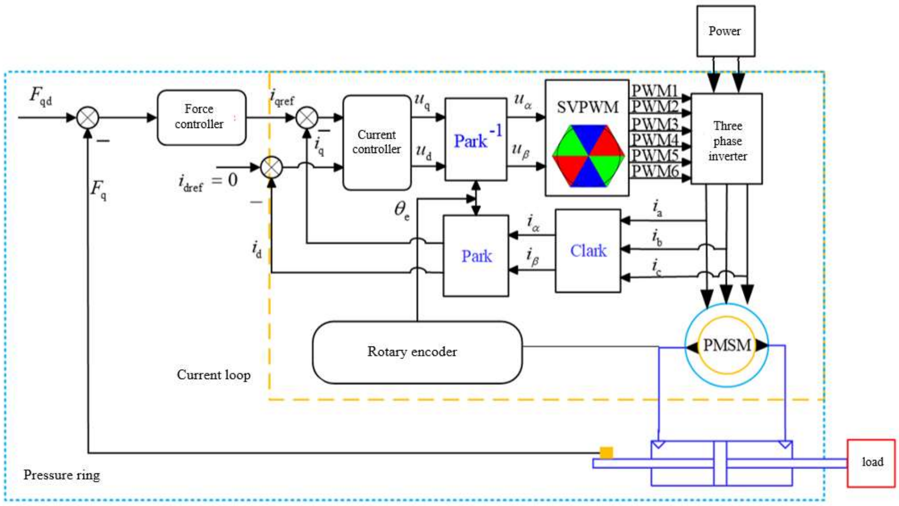

Figure 5. Double closed-loop diagram of force control of the pump control system.

The dynamic performance of an electro-hydraulic servo pump control system is the core to achieve high performance control, which includes the dynamic characteristics of the current loop, speed loop, position loop, and pressure loop. The dynamic characteristics of each link are analyzed in detail below.

4.1. Analysis of the Dynamic Characteristics of Current Loop

The current loop is the innermost loop of the electro-hydraulic servo pump control system, and its core task is to make the current of the motor winding accurately follow the current control instructions. Its performance will directly affect the performance of the outer loop. The closed-loop control structure of the current loop is shown in Figure 6.

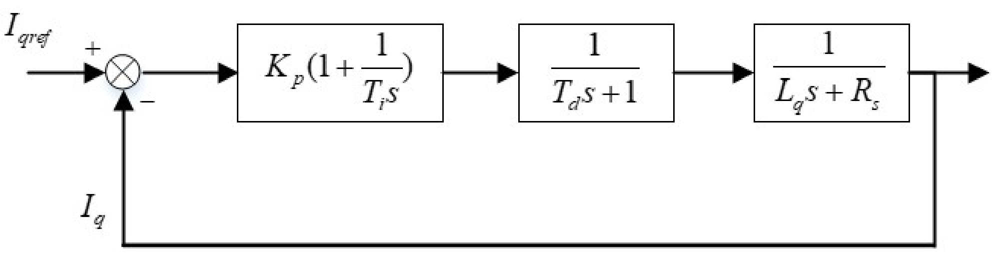

Figure 6. Current loop control diagram of the electro-hydraulic servo pump control system.

Since the time constant of the delay link is far less than that of the controlled object, the system uses first-order inertia to approximate the delay link, and the servo motor current loop usually adopts PI controller.

The open loop transfer function of current loop is:

$$G_0(s) = \frac{K_\mathrm{p}(T_\mathrm{i}s+1)}{T_\mathrm{i}s(T_\mathrm{d}s+1)(L_\mathrm{q}s+R_\mathrm{s})} = \frac{K_\mathrm{p}K_\mathrm{m}(T_\mathrm{i}s+1)}{T_\mathrm{i}s(T_\mathrm{d}s+1)(T_\mathrm{m}s+1)} \tag{7}$$

where $T_\mathrm{m} = L_\mathrm{q}/R_\mathrm{s}$, $K_\mathrm{m} = 1/R_\mathrm{s}$. Because T_m is much larger than T_d, poles with large time constants are eliminated by zero-pole cancellation. The specific PI control parameters can be set as follows:

$$T_\mathrm{i} = T_\mathrm{m} \tag{8}$$

The closed-loop transfer function of the current loop is:

$$G_1(s) = \frac{\frac{K_\mathrm{p}}{L_\mathrm{q}T_\mathrm{d}}}{s^2 + \frac{1}{T_\mathrm{d}}s + \frac{K_\mathrm{p}}{L_\mathrm{q}T_\mathrm{d}}} \tag{9}$$

The system damping ratio and undamped natural frequency are:

$$\begin{cases} \xi_\mathrm{i} = \frac{1}{2}\sqrt{\frac{L_\mathrm{q}}{K_\mathrm{p}T_\mathrm{d}}} \\ \omega_\mathrm{i} = \sqrt{\frac{K_\mathrm{p}}{L_\mathrm{q}T_\mathrm{d}}} \end{cases} \tag{10}$$

The bandwidth frequency defined according to the closed-loop frequency characteristics is the corresponding frequency of -3 dB:

$$\omega_\mathrm{ic} = \omega_\mathrm{i}\sqrt{1 - 2\xi_\mathrm{i}^2 + \sqrt{2 - 4\xi_\mathrm{i}^2 + 4\xi_\mathrm{i}^4}} \tag{11}$$

The damping ratio of the second-order system takes into account the problem of moderate overshoot and fast response of the system. The damping ratio is determined as 0.707, and the PI control parameter is obtained:

$$K_\mathrm{p} = \frac{L_\mathrm{q}}{2T_\mathrm{d}} \tag{12}$$

Then, the current loop bandwidth is:

$$\omega_\mathrm{ic} = \frac{\sqrt{2}}{2T_\mathrm{d}} \tag{13}$$

Therefore, the total delay in the current loop is inversely proportional to the bandwidth of the current loop. Reducing the delay of the current loop can improve the cut-off frequency of the current loop, thus improving the dynamic performance of the current loop.

Based on the working principle and mathematical model of the servo motor, the servo motor vector control block diagram given in Figure 4 is transformed, and the servo motor simulation model is built in the MATLAB/Simulink environment, as shown in Figure 7. In the figure, * represents the expected value.

In the process of Simulink simulation, model parameter setting is a very important part. In order to ensure that the established simulation model is close to the actual system, the system current loop parameters are obtained according to the above current loop analysis and combined with the component technical samples, as shown in Table 1.

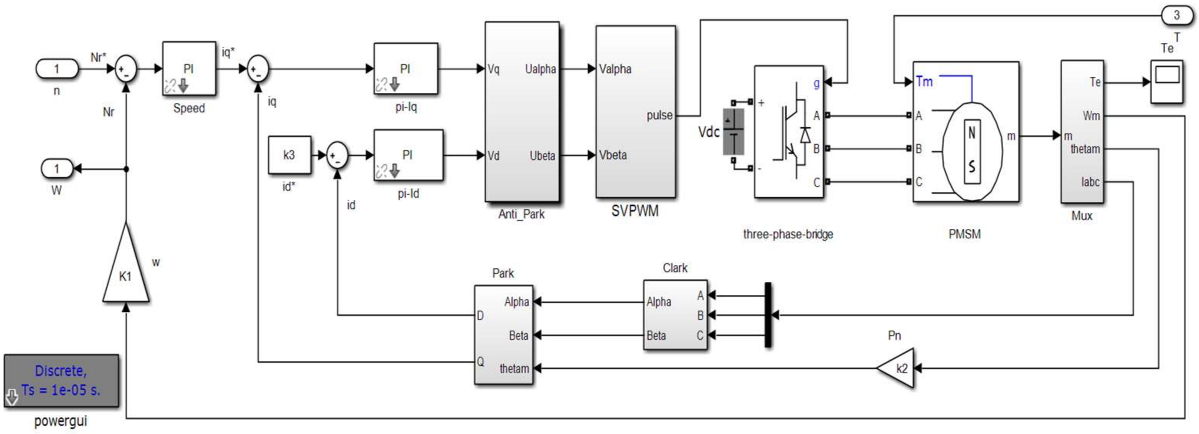

Figure 7. Servo motor vector control simulation model.

Table 1. Current loop simulation model parameters.

Parameter	Physical Meaning	Value
R_s [Ω]	Winding resistance of servo motor	1.1
L_q [H]	Servo motor q-axis inductance	1.87×10^{-2}
L_d [H]	Servo motor d-axis inductance	5.25×10^{-2}
T_d	Time constant of delay link	3×10^{-4}
K_p	Proportional gain	31.16
T_i	Integral time constant	1.7×10^{-2}

The current closed-loop characteristics of the servo motor are simulated and analyzed. The Bode diagram of the current closed-loop frequency characteristics is shown in Figure 8.

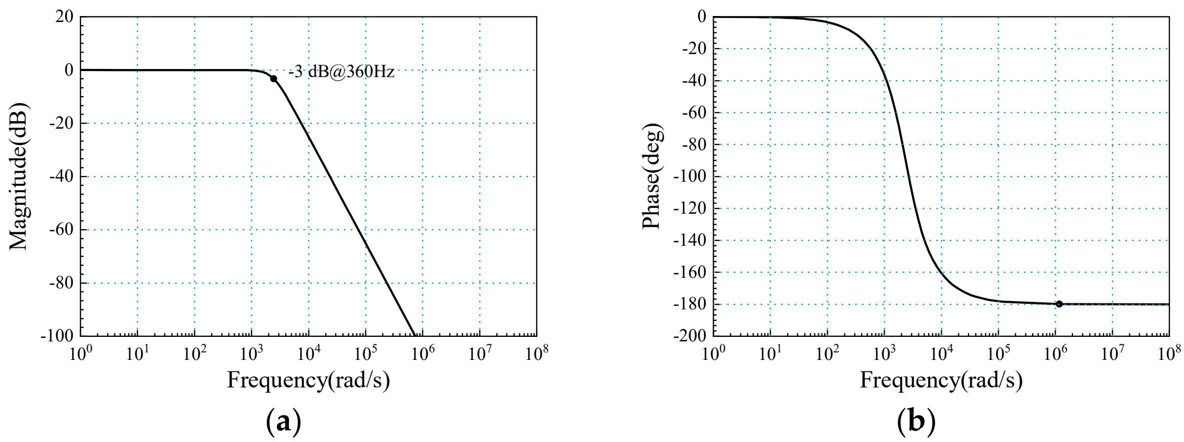

Figure 8. System current loop frequency characteristic curve. (**a**) Amplitude diagram. (**b**) The phase diagram.

Figure 8 shows that after the dynamic analysis and parameter adjustment of the current loop, the bandwidth of the system's current loop can reach 360 Hz. The current loop has a very strong response speed and can quickly track the instruction input signal.

4.2. Analysis of the Dynamic Characteristics of the Speed Loop

The speed loop is the intermediate link of position control in an electro-hydraulic servo pump control system. The core task of the speed loop is to realize volume servo control of the hydraulic system flow indirectly by controlling the speed of the servo motor. A dynamic block diagram of the servo motor speed control is shown in Figure 9.

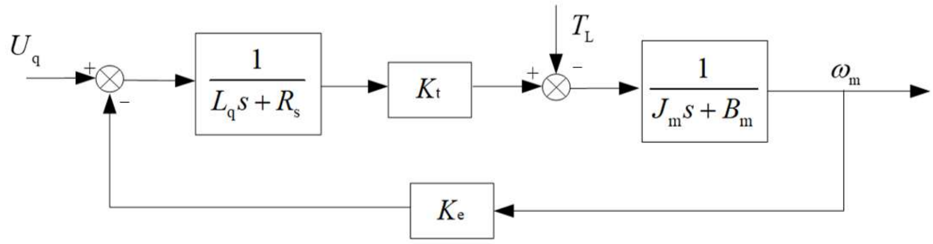

Figure 9. Servo motor dynamic block diagram.

Based on the logic relation of high-frequency dynamics, the bandwidth of the inner current loop is much larger than that of the speed loop; therefore, the current loop as the inner current loop can be degraded, and the current loop as a whole is equivalent to a first-order inertia link:

$$G_1(s) = \frac{1}{\frac{L_q T_d}{K_p}s^2 + \frac{L_q}{K_p}s + 1} \approx \frac{1}{\frac{L_q}{K_p}s + 1} = \frac{1}{\frac{1}{K_i}s + 1} = \frac{1}{T_I s + 1} \tag{14}$$

where K_i is the cut-off frequency after current loop correction. The speed loop usually adopts the PI controller; the control block diagram of the simplified system speed loop is shown in Figure 10.

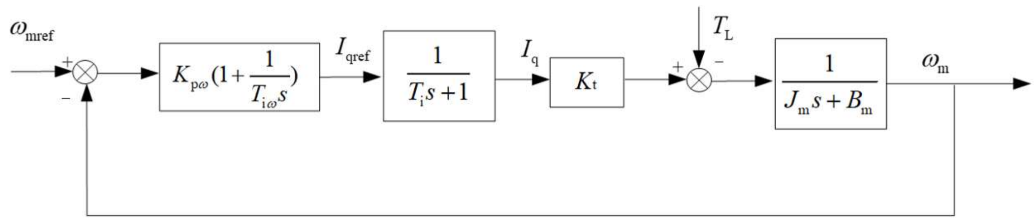

Figure 10. Simplified control chart for the speed loop.

Since B_m is generally much smaller than J_m, damping friction torque can be ignored in design, and the open-loop transfer function of the system can be expressed as:

$$G_{\omega 0}(s) = \frac{K_{p\omega} K_t (T_{i\omega} s + 1)}{J_m T_{i\omega} s^2 (T_I s + 1)} = \frac{K_{\omega 0}(T_{i\omega} s + 1)}{s^2 (T_I s + 1)} \tag{15}$$

The above equation is the open-loop transfer function of a typical type II system, and the open-loop Bode diagram of rotational speed can be obtained as in Figure 11.

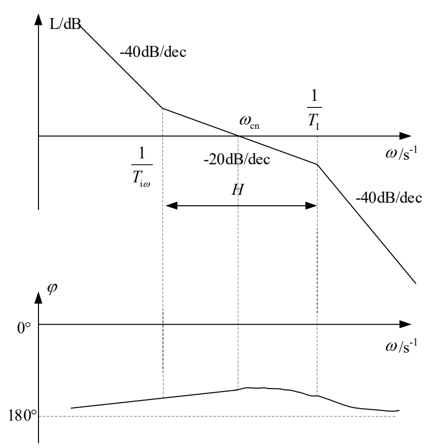

Figure 11. Open-loop Bode diagram of rotational speed.

Defining H as the width of the mid-frequency band (slope of the curve is -20 dB/dec). According to the minimum resonance peak method of a second-order system, the relation between controller parameters and H can be obtained:

$$\begin{cases} T_{\mathrm{i}\omega} = HT_{\mathrm{I}} \\ K_{\omega 0} = \dfrac{H+1}{2H^2T_{\mathrm{I}}^2} \end{cases} \tag{16}$$

At this point, $\omega_{\mathrm{cn}} = \frac{1}{2}(\frac{1}{T_{\mathrm{I}}} + \frac{1}{T_{\mathrm{i}\omega}})$, the relationship among low frequency turning frequency $\omega_{\mathrm{i}0} = 1/T_{\mathrm{i}\omega}$, shear frequency ω_{cn}, and gain $K_{\omega 0}$ is:

$$K_{\omega 0} = \omega_{\mathrm{i}0}\omega_{\mathrm{n}\omega} \tag{17}$$

The shear frequency ω_{cn} can be expressed as:

$$\omega_{\mathrm{cn}} = \frac{H+1}{2HT_{\mathrm{I}}} \tag{18}$$

The parameters in the rotational speed PI controller can be set as:

$$\begin{cases} T_{\mathrm{i}\omega} = HT_{\mathrm{I}} \\ K_{\mathrm{p}\omega} = \dfrac{J_{\mathrm{m}}(H+1)}{2K_{\mathrm{t}}HT_{\mathrm{I}}} \end{cases} \tag{19}$$

According to the above analysis and component technology samples, the system speed loop parameters are obtained, as shown in Table 2.

Table 2. Speed loop simulation model parameters.

Parameter	Physical Meaning	Value
K_{t} [N·m/A]	Motor torque coefficient	0.23
J_{m} [kg·m^2]	Motor pump moment of inertia	8.8×10^{-4}
H	Intermediate frequency bandwidth	1000
$K_{\mathrm{p}\omega}$	Proportional gain	3.19
$T_{\mathrm{i}\omega}$	Integral time constant	0.6

After the mechanical parameters of the motor are put in, the Bode diagram of speed loop frequency characteristics can be obtained as shown in Figure 12. It can be seen that the speed loop bandwidth of the system can reach 110 Hz, and the speed loop has a strong response speed, which can effectively track the instruction input signal.

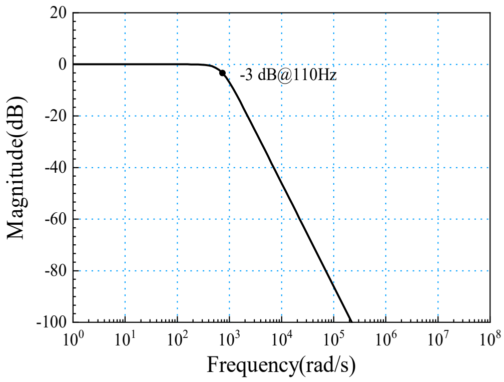

(**a**)

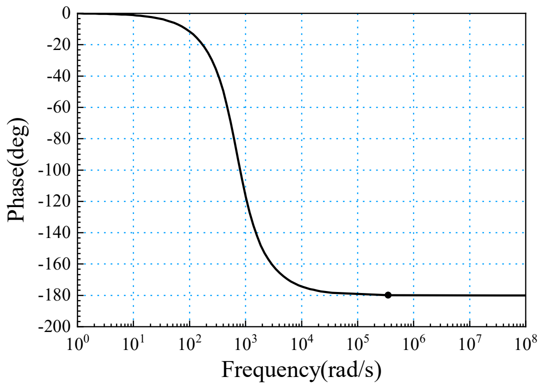

(**b**)

Figure 12. Speed loop closed-loop Bode diagram. (**a**) Amplitude diagram. (**b**) The phase diagram.

4.3. Analysis of the Dynamic Characteristics of Position Loop

Because the servo motor has good dynamic performance and fast response speed, its closed-loop bandwidth is usually much larger than other parts of the hydraulic system. Therefore, the speed loop of the servo motor is simplified as a proportional link:

$$\omega_{\mathrm{p}} = K_{\mathrm{m}} u_{\mathrm{c}} \tag{20}$$

where ω_{p} is the motor output speed, K_{m} is the control gain, and u_{c} is the voltage input signal.

The position loop control structure is shown in Figure 13.

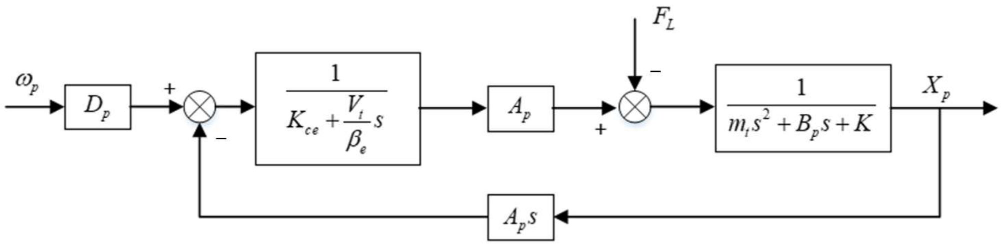

Figure 13. Position loop simplified control diagram.

In many cases, the load of the servo system is mainly inertial load, and the elastic load is very small and can be ignored. In this case, the position loop transfer function can be simplified as:

$$X_{\mathrm{p}} = \frac{\dfrac{D_{\mathrm{p}}\omega_{\mathrm{p}}}{A_{\mathrm{p}}(1+\dfrac{B_{\mathrm{p}}K_{\mathrm{ce}}}{A_{\mathrm{p}}^2})} - \dfrac{K_{\mathrm{ce}}}{A_{\mathrm{p}}^2 + B_{\mathrm{p}}K_{\mathrm{ce}}}\left(1+\dfrac{V_{\mathrm{t}}}{4\beta_{\mathrm{e}}K_{\mathrm{ce}}}s\right)F_{\mathrm{L}}}{s(\dfrac{s^2}{\omega_{\mathrm{nc}}^2}+\dfrac{2\zeta_{\mathrm{nc}}}{\omega_{\mathrm{nc}}}s+1)} \tag{21}$$

The natural frequency and damping ratio of the position loop can be expressed as:

$$\begin{cases} \omega_{\mathrm{nc}} = \sqrt{\dfrac{4\beta_{\mathrm{e}}A_{\mathrm{p}}^2}{m_{\mathrm{t}}V_{\mathrm{t}}}(1+\dfrac{B_{\mathrm{p}}K_{\mathrm{ce}}}{A_{\mathrm{p}}^2})} \\ \zeta_{\mathrm{nc}} = \dfrac{K_{\mathrm{ce}}A_{\mathrm{p}}}{A_{\mathrm{p}}^2 + B_{\mathrm{p}}K_{\mathrm{ce}}}\sqrt{\dfrac{m_{\mathrm{t}}\beta_{\mathrm{e}}}{V_{\mathrm{t}}}} + \dfrac{B_{\mathrm{p}}A_{\mathrm{p}}}{4(A_{\mathrm{p}}^2 + B_{\mathrm{p}}K_{\mathrm{ce}})}\sqrt{\dfrac{V_{\mathrm{t}}}{m_{\mathrm{t}}\beta_{\mathrm{e}}}} \end{cases} \tag{22}$$

According to Equation (21), the dynamic response characteristic transfer function of position output to input ω_{p} is composed of proportion, integral, and second-order oscillation. The main performance parameters are speed amplification factor K_v, hydraulic natural frequency ω_{nc}, and the hydraulic damping ratio ζ_{nc}. Further, the system speed amplification coefficient can be expressed as:

$$K_v = \frac{D_{\mathrm{p}}}{A_{\mathrm{p}}(1+\frac{B_{\mathrm{p}}K_{\mathrm{ce}}}{A_{\mathrm{p}}^2})} = \frac{A_{\mathrm{p}}D_{\mathrm{p}}}{A_{\mathrm{p}}^2 + B_{\mathrm{p}}K_{\mathrm{ce}}} \tag{23}$$

The main performance parameters are analyzed in detail below.

(1) Speed amplification factor

The transfer function contains an integral link; therefore, in the steady state, the output of the hydraulic cylinder piston speed and motor input speed is proportional to the relationship. The proportionality coefficient A represents the sensitivity of the speed of the quantitative pump to the speed of the hydraulic cylinder, which directly affects the stability, response speed, and accuracy of the electro-hydraulic servo pump control system. Increasing the speed amplification coefficient can improve the response speed and accuracy of the system but can deteriorate the stability of the system.

(2) Hydraulic natural frequency

Hydraulic natural frequency is the bottleneck of the whole system, which limits the response speed of the system. In order to improve the response speed of the system, the hydraulic natural frequency should be increased. The specific implementation methods of improving hydraulic natural frequency are as follows:

1. The hydraulic cylinder piston area A_p can be increased to improve the natural frequency of the system, but when the piston area A_p increases, the system needs more flow at the same frequency response speed.
2. The integrated design scheme of EPU, functional valve set, and hydraulic cylinder can be adopted to reduce the specific connection between the oil port of quantitative pump and hydraulic cylinder and reduce the total compression volume V_t.
3. The total leakage coefficient K_{ce} of the system can be increased, but this method will sacrifice the working efficiency of the system and cause an increase in the oil working temperature; therefore, it is not suitable for long-term operation under all working conditions.
4. The total mass m_t converted to the piston can be reduced, increasing the effective bulk elastic modulus β_e of oil.

(3) Hydraulic damping ratio

The hydraulic damping ratio represents the relative stability of the system, which is mainly determined by the total leakage coefficient K_{ce} and viscous damping coefficient B_p. Improving the hydraulic damping ratio is of great significance to improve system performance. Specific methods are as follows:

1. The bypass leakage channel can be set to increase the viscous damping B_p of the load.
2. The quantitative pump and hydraulic cylinder with large leakage coefficients can increase the system damping, but will cause a large power loss, and the nonlinear characteristics of the output flow of the quantitative pump will be further intensified.

4.4. Analysis of the Dynamic Characteristics of the Pressure Loop

Because the servo motor current loop has good dynamic performance and fast response speed, its closed-loop bandwidth is usually much larger than the motor speed loop and other parts of the hydraulic system; therefore, the servo motor current loop in the system can be simplified as a proportional link. We have:

$$i_q = K_n u_c \tag{24}$$

where K_n is the control gain.

The servo motor operates in the current loop, and the EPU is in voltage regulating mode. The system can be described by the following basic equation:

$$\begin{cases} T_e - T_L = J_m \omega_m s + B_m \omega_m \\ Q_p = D_p \omega_m - C_p P_L \\ Q_p = A_p x_p s + K_{ce} P_L + \dfrac{V_t}{4\beta_e} P_L s \\ F_p = A_p P_L = m_t x_p s^2 + B_p x_p s + K x_p \end{cases} \tag{25}$$

The pressure loop control structure is shown in Figure 14.

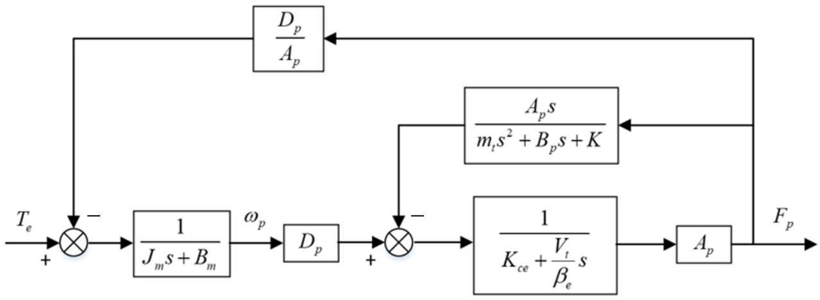

Figure 14. Pressure loop simplified control diagram.

Since the damping coefficient of load is small, B_m and B_p can be ignored, and the open-loop transfer function of the system can be simplified as:

$$G(s)H(s) = \frac{\frac{D_p^2}{J_m K_{ce}}\left(\frac{s^2}{\omega_m^2}+1\right)}{s\left(\frac{s}{\omega_r}+1\right)\left[\frac{s^2}{\omega_0^2}+\frac{2\xi_0 s}{\omega_0}+1\right]} \tag{26}$$

where ω_m is the natural frequency of the load, $\omega_m = \sqrt{K/m_t}$; ω_r is the ratio of series coupling stiffness of hydraulic spring and load spring to damping system, $\omega_r = \frac{C_t}{A_c^2}/\left(\frac{1}{K_h}+\frac{1}{K}\right)$; ω_m is the natural frequency formed by coupling stiffness and load mass, $\omega_0 = \omega_m\sqrt{1+\frac{K_h}{K}}$; ξ_0 is the damping ratio, $\zeta_0 = \frac{1}{2\omega_0}\frac{4\beta_e C_t}{V_t[1+(K/K_h)]}$; K_h is the hydraulic spring stiffness, $K_h = \frac{4\beta_e A_p^2}{V_t}$

Let the open-loop gain of the system be K_0, and the following formula is obtained:

$$K_0 = \frac{D_p^2}{J_m K_{ce}} \tag{27}$$

The open-loop gain of the pressure loop can be improved by increasing quantitative pump displacement D_p, and decreasing motor pump inertia J_m and total leakage coefficient K_{ce}.

(1) When the load stiffness K is much greater than the hydraulic spring stiffness K_h, $\omega_r \approx \frac{K_{ce}K_h}{A_p^2}$, $\omega_0 \approx \omega_m = \sqrt{\frac{K}{m_t}}$. In Equation (26), the second-order oscillation link and the second-order differential link approximately cancel, and the dynamic characteristics of the system are mainly determined by the integral link and the inertia link in series. Cut-off frequency $\omega_c = \frac{D_p^2 K_h}{J_m A_p^2}$, the system cut-off frequency can be improved by increasing the displacement of quantitative pump D_p, reducing the rotational inertia of motor pump group J_m, and reducing the volume of hydraulic cylinder V_t.

(2) When the load stiffness K is far less than the hydraulic spring stiffness K_h, $\omega_r \approx \frac{K_{ce}K}{A_p^2}$, and then $\omega_0 \approx \omega_h = \sqrt{\frac{Kh}{m_t}} \gg \omega_m = \sqrt{\frac{K}{m_t}} > \omega_r$. As K decreases, ω_r, ω_m, and ω_0 all decrease, ω_r and ω_m decrease more; therefore, the distance between ω_m and ω_0 increases, and the resonance peak at ω_0 increases. The cut-off frequency is $\omega_c = \frac{D_p^2 K}{J_m A_p^2}$, and the system cut-off frequency can be improved by increasing the displacement of

quantitative pump D_p, decreasing the moment of inertia of motor pump group J_m, and appropriately increasing the load stiffness K.

5. System Simulation Analysis

Based on the working principle of an electro-hydraulic servo pump control system shown in Figure 1 and combined with the principle analysis of each control loop of the system, the simulation models of a permanent magnet synchronous motor, quantitative pump and hydraulic cylinder, and other components are connected to form the overall simulation model of the electro-hydraulic servo pump control system, as shown in Figure 15.

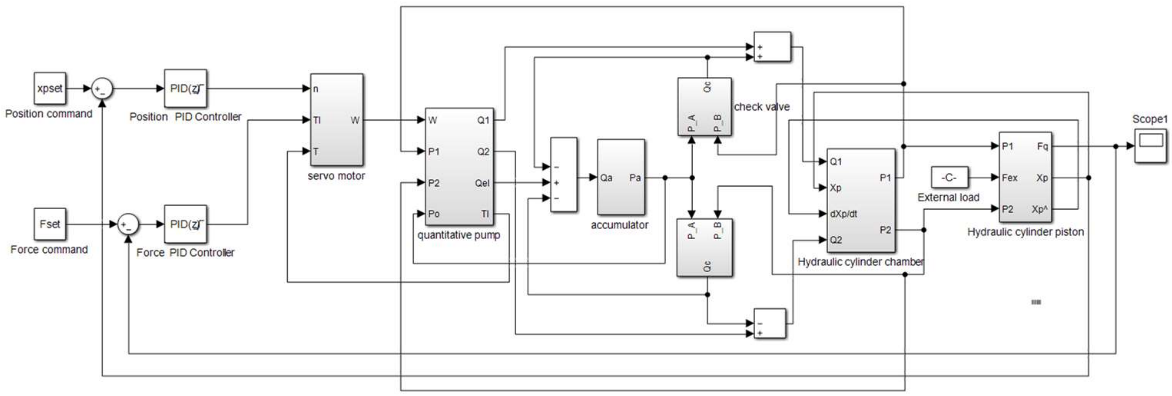

Figure 15. The whole system simulation model.

In the process of Simulink simulation, the model parameter settings are very important. In order to ensure that the established simulation model is close to the actual system, parameter assignment is combined with component technology samples, and other system parameters are obtained, as shown in Table 3.

Table 3. System simulation model parameters.

Parameter	Physical Meaning	Value
C_{ip} [(m^3/s)/Pa]	Internal leakage coefficient of pump	1×10^{-3}
C_{ep} [(m^3/s)/Pa]	External leakage coefficient of pump	1×10^{-3}
D_p [mL/r]	Pump delivery	0.8
C_{ic} [(m^3/s)/Pa]	Internal leakage coefficient of hydraulic cylinder	1×10^{-3}
K_{vp} [N/(m/s)]	Damping coefficient of piston	150
k	Gas polytropic coefficient	1.3
F_s [N]	Sliding static friction	25
F_c [N]	Sliding Coulomb friction	15
V_0 [mL]	Initial volume of one side of hydraulic cylinder	450
β_e [N/m^2]	Oil elastic modulus	6.5×10^8
A [cm^2]	Effective area of piston	71
m [Kg]	Load conversion quality	8.5
V_{gi} [mL]	Initial gas volume of accumulator	800
P_{ai} [MPa]	Initial pressure of accumulator	3
V_{ai} [mL]	Initial oil volume of accumulator	200
u [V]	Rated voltage of servo motor	220
P_m [kW]	Rated power of servo motor	21
n [r/min]	Rated speed of servo motor	3000
T_e [N·m]	Servo motor torque	22
K_e [V/(rad/s)]	Servo motor counter electromotive force	1.03×10^2

PID controllers have been widely used in electro-hydraulic servo control systems due to their simple structure and strong robustness. Therefore, in order to verify the rationality and correctness of the mechanism model and the simulation model of the electro-hydraulic servo pump control system established in this paper, a PID controller was adopted. The parameters of the PID controller were adjusted by the trial-and-error method. Finally, the PID controller gain P of the position control system is 52.5, the gain I is 5, and the gain D is 0; the gain P of the PID controller of the force control system is 43, the gain I is 3, and the gain D is 0.

Given the typical step signal and sinusoidal signal of the system, the position closed-loop control and force closed-loop control of the system are simulated and analyzed, respectively. The simulation results are shown in Figures 16 and 17.

Figure 16 shows that the displacement of the hydraulic cylinder can basically follow the expected position instruction. When the expected position instruction is 0–15 mm step, the position reaches a steady state after 2 s, and the steady-state error is about ±0.05 mm. When the expected position instruction is ±2 mm @ 0.5 Hz sine, the position following has a certain amplitude and phase lag. The position error of dynamic tracking reaches 0.5 mm, and the phase lag is within the range of ±10°.

It can be seen from Figure 17 that the output force of the hydraulic cylinder can basically follow the expected force command. When the expected force command is 0–6.28 kN step, the output force of the hydraulic cylinder has a certain overshoot, the output reaches steady state after 2.5 s, and the steady-state error of output force is about ±0.1 kN. When the expected position command is ±0.3 kN @ 1 Hz sine, the force output follows a certain amplitude attenuation. The error of dynamic following force is ±0.15 kN.

Based on the above analysis, it can be seen that the electro-hydraulic servo pump control system using a simple PID controller for simulation control can follow the instructions well, which verifies that the system has good position and force control performance after the dynamic analysis and parameter determination of the system control loop.

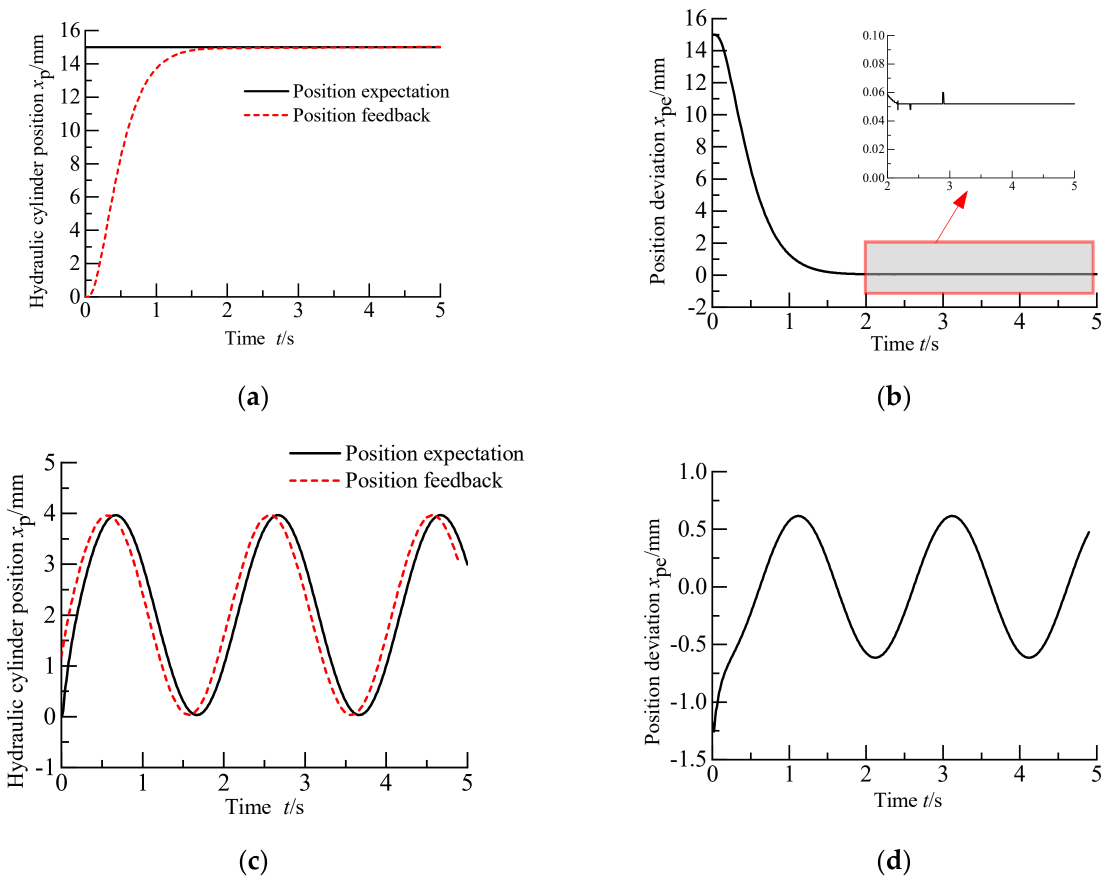

Figure 16. Simulation curve of position control. (**a**) Step position response curve. (**b**) Step position error curve. (**c**) Sinusoidal position response curve. (**d**) Sinusoidal position error curve.

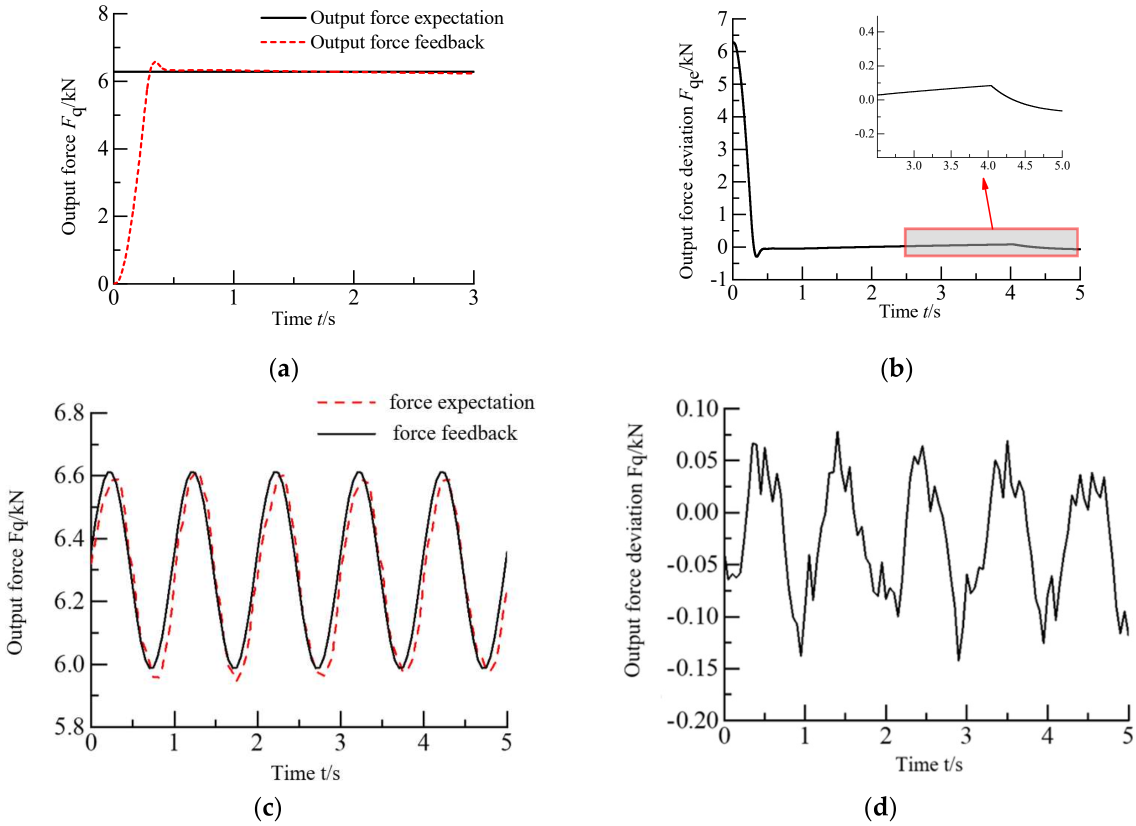

Figure 17. Simulation curve of force control. (**a**) Step output force response curve. (**b**) Step output force error curve. (**c**) Sinusoidal output force response curve. (**d**) Sinusoidal output force error curve.

6. Experimental Study

6.1. Electro-Hydraulic Servo System Test Bench Design

The experiment in this paper relies on the enterprise research and development project "Gas Turbine Adjustable Guide Vane Electro-Hydraulic Servo Pump Control System" and builds an electro-hydraulic servo pump control experimental platform. The experimental platform uses the load cylinder to load the experimental cylinder. The experimental platform is mainly composed of an upper computer PLC, a Hollysys motion controller, a servo driver, a motor pump unit, a functional valve block, an experimental and loading hydraulic cylinder, an electric control cabinet operation console, etc. The structure of the experimental platform is shown in Figure 18.

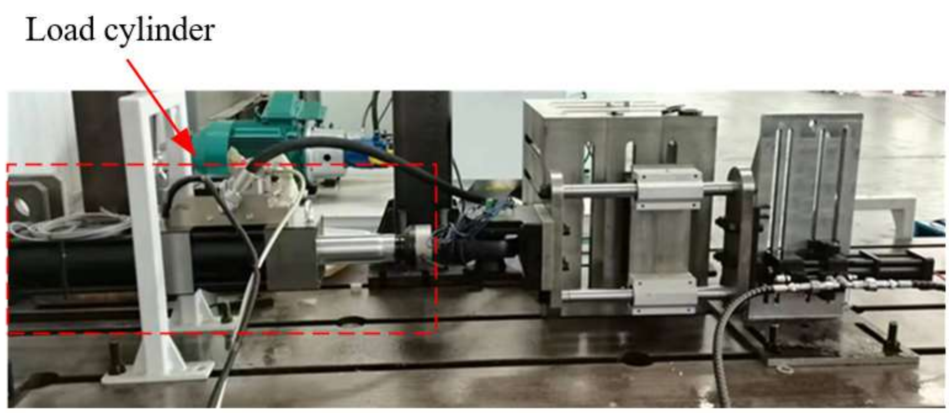

(**a**)

Figure 18. *Cont.*

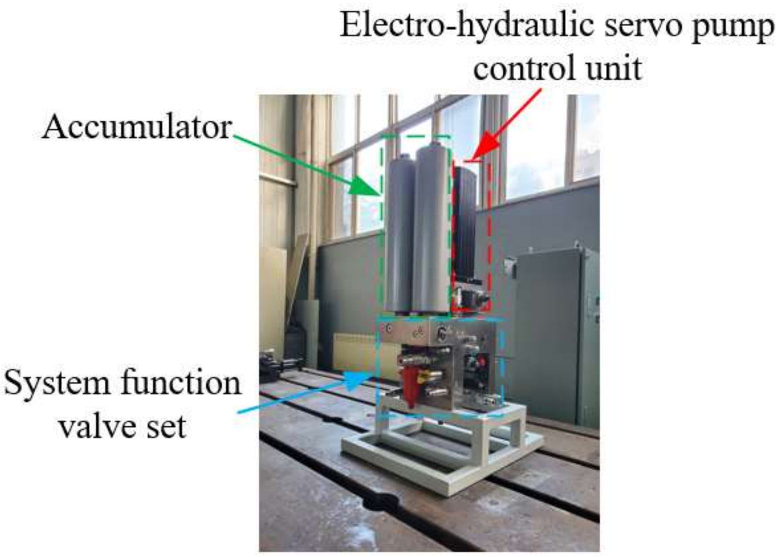

(**b**)

Figure 18. System test platform. (**a**) Hydraulic cylinder loading platform. (**b**) Pump control integrated unit.

The upper computer PLC sends the control command to the Hollysys motion controller through the analog quantity. At the same time, the controller collects the pressure, displacement, temperature, and other information in the hydraulic system in real time through the sensor, obtains the control output signal combined with the PID control algorithm program, sends the output signal to the servo driver, then controls the action of the motor pump unit, and finally realizes the accurate control of the hydraulic system, which realizes the high-performance closed-loop control.

6.2. Experimental Study and Result Analysis

The specific implementation methods of the experiment are as follows. Firstly, edit the system logic control program in the Hollysys programming software AutoThink. Then, give the periodic expected signal command through the software program (here we use the step response signal). The PID controller is used to control the position and force of the system, and the displacement signal of the displacement sensor and the force signal of the force sensor are collected and analyzed in real time. Finally, the actual position and output of the system are obtained.

6.2.1. Position Control Experiment

Given the position step signal from 30 mm to 80 mm, the response curve of the system position is shown in Figure 19, and the error curve of the position is shown in Figure 20.

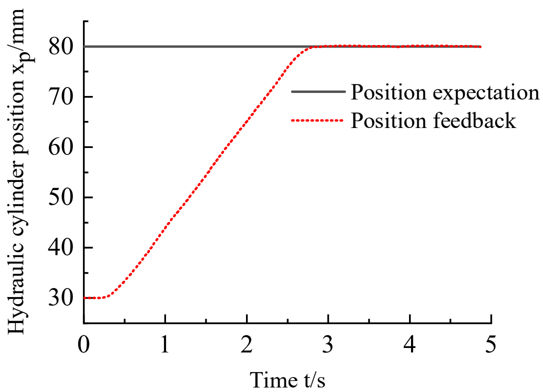

Figure 19. Response curve of step position.

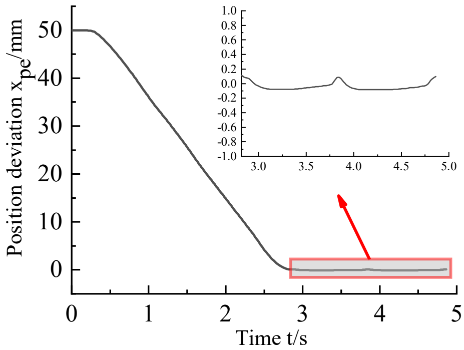

Figure 20. Error curve of step position.

It can be seen from the above two figures that when the desired position command is 30–80 mm, the displacement of the hydraulic cylinder can basically follow the desired position command in the dynamic response. After 2.8 s, the position of the hydraulic cylinder reaches a steady state, and the steady-state error of the position is about ±0.1 mm.

6.2.2. Force Control Experiment

Given the step signal from 10 kN to 20 kN, the response curve of the system output force is shown in Figure 21, and the error curve of the force is shown in Figure 22.

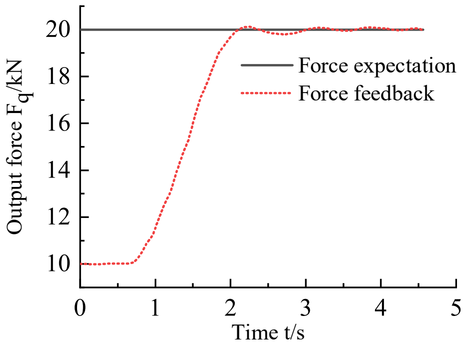

Figure 21. Response curve of step force.

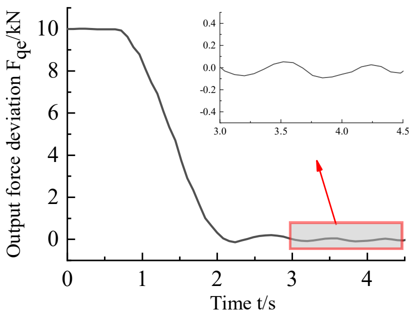

Figure 22. Error curve of step force.

It can be seen from the above two figures that when the current expected force command is 10–20 kN, the output force of the hydraulic cylinder can basically follow the expected force command in the dynamic response. After 3 s, the output of the hydraulic cylinder reaches a steady state, and the steady-state error of the output force is about ±0.2 kN.

Based on the above analysis, after the dynamic analysis and parameter determination of the system control loop, the electro-hydraulic servo pump control system has good dynamic response performance and stable accuracy in the process of hydraulic cylinder position and output force control on the test bench. The position control accuracy can reach ± 0.1 mm and the force control accuracy can reach ± 0.2 kN.

7. Conclusions

Aiming at the problems of low static accuracy and limited dynamic performance of an electro-hydraulic servo pump control system due to electromechanical hydraulic coupling, flow nonlinearity, and other factors, the dynamic response characteristics of current loop, speed loop, position loop, and pressure loop are analyzed, and the following conclusions are obtained:

(1) The principle of an electro-hydraulic servo pump control is introduced, and a mathematical model of an electro-hydraulic servo pump control system is established.
(2) Based on the logical relationship of high-frequency dynamics, starting with the current inner loop with faster response, the dynamic characteristics of each control loop are analyzed, and the parameter values are determined in combination with the technical samples of components. The Simulink position/force simulation model of the system is built. The simulation results show that the system has good position and force control performance after the dynamic analysis of the system control loop and the determination of component parameters.
(3) The experimental results show that the system parameter determination, based on the dynamic analysis of the system control loop proposed in this paper, can make the system achieve good dynamic response effect and steady-state accuracy of position/force control. However, the nonlinear mathematical model of the system is partially idealized and simplified. In order to further improve the nonlinear accuracy of the system, the nonlinear model can be further refined.

Author Contributions: Conceptualization, W.J. and P.J.; methodology, G.C.; experiment and analysis, G.Y. and C.J.; software, P.J.; investigation, W.J.; writing—original draft preparation, T.Z. and K.L.; writing—review and editing, W.S. and G.Y.; project administration, C.A.; funding acquisition, G.C. All authors have read and agreed to the published version of the manuscript.

Funding: This research was supported by the Key R&D Projects in Hebei Province (no. 20314402D), the Key Project of Science and Technology Research in Hebei Province (no. ZD2020166), the Key Project of Science and Technology Research in Hebei Province (no. ZD2021340), the General Project of Natural Science Foundation in Xinjiang Uygur Autonomous Region (no. 2021D01A63), the Project supported by the Natural Science Foundation of Xinjiang Uygur Autonomous Region (2022D01A51) and the Project of Scientific Research Plan of Colleges and Universities in Xinjiang Uygur Autonomous Region (XJEDU2021Y050).

Conflicts of Interest: The authors declare no conflict of interest.

References

1. Bo, W.; Yunxiao, H.; Long, Q.; Xiangyu, W.; Lei, G.; Bin, Z. Research on characteristics of electro hydraulic servo system controlled by separate cavity independent variable speed pump. *Mech. Eng.* **2020**, *56*, 235–243. [CrossRef]
2. Zhao, P. *Research on Position Control of Transferable Vane Electro-Hydraulic Servo Closed Pump Control System*; Yanshan University: Yanshan, China, 2020.
3. Merritt, H.E. Hydraulic Control System. *J. Appl. Mech.* **1967**, *35*, 31–32. [CrossRef]
4. Nakano, K.; Tanaka, Y. Energy saving type electro-hydraulic servo system. *J. Fluid Control* **1988**, *18*, 35–51.
5. Xu, S. Three stages of hydraulic transmission control system development from energy saving perspective. *Hydraul. Pneum. Seals* **2005**, *4*, 24–31.
6. Alden, R. C-141 and C-130 power-by-wire flight control systems. In Proceedings of the IEEE 1991 National Aerospace and Electronics Conference, Dayton, OH, USA, 20–24 May 1991; Volume 2, pp. 535–539.
7. Sedrak, D. Closed-loop electronic valuing and the application of variable voltage variable frequency in hydraulics. *Elev. World* **1999**, *47*, 66–72.
8. Jawaid, S.I.; Wang, L. EHA System Integration Design Analysis and Position Tracking Performance by PID Controller. *Appl. Mech. Mater.* **2013**, *419*, 826–834. [CrossRef]
9. Han, R. Discussion on the technology of aviation electro-hydraulic actuator. *Sci. Technol. Horiz.* **2019**, *12*, 34–35.

10. Den, D.V.; Airbus, B. The A380 Flight control electro hydrostatic actuators—Achievements and lessons learnt. In Proceedings of the 25th Congress of the International Council of the Aeronautical Sciences, Hamburg, Germany, 3–8 September 2006; Volume 6.
11. Chakraborty, I.; Mavris, D.N.; Emeneth, M.; Schneegans, A. A system and mission level analysis ofelectrically actuated flight control surfaces using Pacelab SysArc. In Proceedings of the AIAA science and technology forum and exposition (SciTech 2014), National Harbor, MD, USA, 13–17 January 2014; pp. 1–22.
12. Guo, X.; Wang, C.; Liu, H. Sliding mode control of pump controlled electro-hydraulic servo system based on extended observer. *J. Beijing Univ. Aeronaut. Astronaut.* **2020**, *7*, 1–12.
13. Fu, J.; Maré, J.C.; Fu, Y. Modelling and simulation of flight control electromechanical actuators with special focus on model architecting, multidisciplinary effects and power flows. *Chin. J. Aeronaut.* **2017**, *30*, 47–65. [CrossRef]
14. Vasiliu, N.; Vasiliu, D.; Călinoiu, C.; Puhalschi, R. *Simulation of Fluid Power Systems with Simcenter Amesim*; CRC Press: Boca Raton, FL, USA, 2018.
15. Yu, A.; Li, Y.; Wang, C.; Jiang, J.; Yan, C. Research on electro-hydraulic servo system of direct drive single output rod symmetrical hydraulic actuator. *Hydraul. Pneum.* **2017**, *2*, 27–32.
16. Kim, J.H.; Hong, Y.S. Robust internal-loop compensation of pump velocity controller for precise force control of an electro-hydrostatic actuator. *J. Drive Control* **2018**, *15*, 55–60.
17. Liem, D.T.; Truong, D.Q.; Park, H.G. A Feedforward Neural Network Fuzzy Grey Predictor-based Controller for Force Control of an Electro-hydraulic Actuator. *Int. J. Precis. Eng. Manuf.* **2016**, *17*, 309–321. [CrossRef]
18. Deticek, E.; Kastrevc, M. Design of Lyapunov Based Nonlinear Position Control of Electrohydraulic Servo Systems. *J. Mech. Eng.* **2016**, *62*, 163–170. [CrossRef]
19. Soon, C.C.; Ghazali, R.; Jaafar, H.I. Sliding Mode Controller Design with Optimized PID Sliding Surface Using Particle Swarm Algorithm. *Procedia Comput. Sci.* **2017**, *105*, 235–239. [CrossRef]
20. Suzuki, R.; Komagata, M.; Ko, T. Development of 3-DOF wrist mechanism for electro-hydrostatically driven robot arm. *Adv. Robot.* **2020**, *34*, 958–973. [CrossRef]
21. Ko, T.H.; Kaminaga, H.; Nakamura, Y. Key design parameters of a few types of electro-hydrostatic actuators for humanoid robots. *Adv. Robot.* **2018**, *32*, 1241–1252. [CrossRef]
22. Fu, Y.; Yan, M. Research on sliding mode variable structure control of electromechanical actuator for loading system. *Hydraul. Pneum.* **2017**, *2*, 75–80.
23. Altare, G.; Vacca, A. A Design Solution for Efficient and Compact Electro-hydraulic Actuators. *Procedia Eng.* **2015**, *106*, 8–16. [CrossRef]
24. Fu, Y.; Han, X.; Sepehri, N. Design and Performance Analysis of Position-based Impedance Control for an Electrohydrostatic Actuation System. *Chin. J. Aeronaut.* **2018**, *31*, 584–596. [CrossRef]
25. Kang, R.; Jiao, Z.; Mare, J.C. Nonlinear block diagram modeling and robust control method of electro-hydraulic actuator. *J. Aeronaut.* **2009**, *30*, 518–525.
26. Li, Z.; Shang, Y.; Jiao, Z. Analysis of the Dynamic Performance of an Electro-hydrostatic Actuator and Improvement Methods. *Chin. J. Aeronaut.* **2018**, *31*, 2312–2320. [CrossRef]